

Online Video Quality Enhancement with Spatial-Temporal Look-up Tables

Zefan Qu
Tongji University
qzf@tongji.edu.cn

Xinyang Jiang
Microsoft Research Asia
xinyangjiang@microsoft.com

Yifan Yang
Microsoft Research Asia
yifanyang@microsoft.com

Dongsheng Li
Microsoft Research Asia
dongsheng.li@microsoft.com

Cairong Zhao*
Tongji University
zhaocairong@tongji.edu.cn

Abstract

Low latency rates are crucial for online video-based applications, such as video conferencing and cloud gaming, which make improving video quality in online scenarios increasingly important. However, existing quality enhancement methods are limited by slow inference speed and the requirement for temporal information contained in future frames, making it challenging to deploy them directly in online tasks. In this paper, we propose a novel method, *STLVQE*, specifically designed to address the rarely studied online video quality enhancement (Online-VQE) problem. Our *STLVQE* designs a new VQE framework which contains a Module-Agnostic Feature Extractor that greatly reduces the redundant computations and redesign the propagation, alignment, and enhancement module of the network. A *Spatial-Temporal Look-up Tables (STL)* is proposed, which extracts spatial-temporal information in videos while saving substantial inference time. To the best of our knowledge, we are the first to exploit the LUT structure to extract temporal information in video tasks. Extensive experiments on the MFQE 2.0 dataset demonstrate that our *STLVQE* achieves a satisfactory performance-speed trade-off.

1. Introduction

With the rapid development of social media, users are increasingly seeking high-quality and real-time video content. In recent times, video-based applications such as video conferencing, webcasting, and cloud gaming have increasingly demanded low latency requirements. This has resulted in higher video compression rates, which can cause a noticeable decrease in video quality and an overall reduction in the Quality of Experience (QoE). As a result, online Video Quality Enhancement (Online-VQE), which improves the quality of real-time streaming video under online conditions and minimizing video defects caused by compression algo-

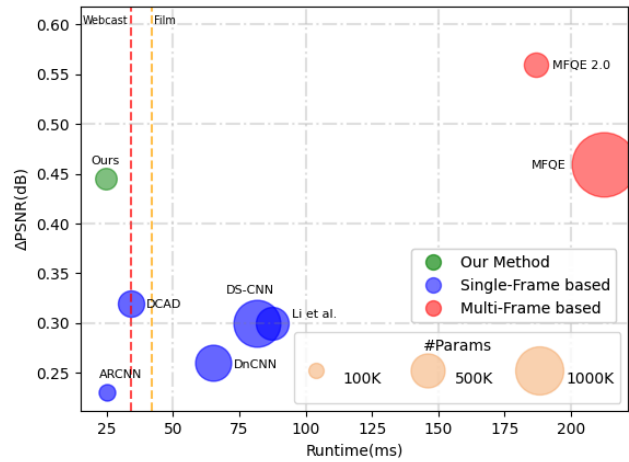


Figure 1. Comparison of PSNR, average runtime per frame(720P video) and parameters on MFQE 2.0 test set at QP=37. Our *STLVQE* method achieves a great trade-off in enhancement performance and inference speed.

rithms (e.g., H.264/AVC [28] and H.265/HEVC [25]) has become a significant problem. However, Online-VQE poses two main challenges compared to the conventional offline VQE approach. Firstly, it needs to process high-resolution videos in real-time to ensure a smooth viewing experience. Secondly, online video processing techniques [15, 18, 22] can only rely on the current and previous frames for inference due to the uncontrolled latency caused by waiting for future frames, which can result in overall video delay.

In recent years, numerous neural network-based techniques for enhancing the quality of compressed video have been developed, resulting in significant advancements in this field. These methods can be broadly classified into two categories, namely single-image based VQE method [4, 12, 30, 31] and multi-frame based VQE method [2, 6, 10, 20, 36]. Single-image based approaches are relatively faster in inference speed, but they ignore the significance of tempo-

ral information in video [32]. On the other hand, multi-frame based VQE achieves state-of-the-art performance by utilizing temporal information. However, most of these approaches are not suitable for online scenarios because they rely on subsequent frames as reference frames and have unsatisfactory inference speeds. Therefore, developing a new online-VQE method that satisfies the aforementioned two constraints while effectively leveraging temporal information is essential.

Reasons that limit the speed and latency of the above temporal VQE methods can be summarized in the following two points: First, a high level of computational redundancy exists within these methods, and these homogeneous computations increase the network’s inference time. Second, most of these methods employ complex and computationally intensive models, which sacrificing inference speed and latency for some of the enhancement capabilities. In this work, a more applicable VQE method for online scenarios are proposed by advancing these two perspectives.

As discussed in previous works [1], modern VQE methods exploit temporal information by constructing a neural network containing three main components: the propagation, alignment and enhancement module. In all three modules, similar feature extraction operations on the original image may be involved, e.g., the reference frame selection [10, 32] in propagation module, the optical flow calculation [1, 2] in alignment module and the final result obtaining in the enhancement module [6, 10]. Most of the state-of-the-art methods adopts distinct feature extractors in different components and obtaining latent feature for each component separately, causing large computation redundancy. In this paper, we design a new VQE network framework containing a Module-Agnostic Feature Extractor (MAFE), where the extracted latent feature are uniformly share across three modules. This design allows the network to greatly reduce the redundant feature computation steps and speed up the inference of the network.

When processing high-resolution videos in VQE task, the complex network of the sota method will greatly increase the computation times of the network, thus affecting the online deployment of the method. Therefore, we in our proposed framework: (1) Redesign the structure of the three modules with a light-weight convolutional structure. (2) A Spatial-Temporal Look-up Tables (ST-LUTs) that extend conventional LUTs [13] to conduct queries on both spatial and temporal dimensions is proposed, which allows the LUTs to simultaneously capture information in both temporal and spatial dimensions, facilitating efficient extraction of temporal information. To the best of our knowledge, ST-LUTs is the first approach to employ a LUT structure for the extraction of temporal information.

The major contributions are summarized as follows: (1) We propose the first online-VQE method STLVQE that

achieves real-time process speed, which reduces redundant feature extraction computations while redesigning the propagation, alignment and enhancement modules of the temporal VQE network. (2) A Spatial-Temporal Look-up Table structure is first time proposed for fully exploiting the temporal and spatial information in the video. (3) Extensive qualitative and quantitative experiments on Compressed VQE benchmark dataset MFQE 2.0 demonstrate that our approach achieves a comparable speed-performance trade-off.

2. Related Work

Compressed Video Quality Enhancement. Recently, numerous works have focused on the degradation of the network video quality due to the lossy video compression algorithms. Existing Compressed VQE work can be broadly classified into two categories, which are single-image based method [4, 5, 8, 11, 12, 17, 30, 34] and multi-frame based method [2, 6, 7, 10, 20, 29, 32, 36].

For the single-image based methods, some of the early work [4, 8, 11, 17, 31, 34] are mainly used to enhance the quality of JPEG compressed images, which can also be applied directly to compressed videos to process each frame independently. [5, 12, 30] utilize certain characteristics of the video compression algorithm or compression parameters to improve the video quality. For example, DS-CNN [30] and QE-CNN [31] use distinct models to enhance the video processed by different compression coding.

For the multi-frame based methods, MFQE 1.0 [32] and MFQE 2.0 [10] were proposed to use two adjacent high quality frames(PQF) and compute the optical flow between them to enhance the current frame. STDF [6] uses deformation convolution for an implicit alignment. RFDA [36] extracts long-range temporal information from the video via the recursive fusion module. BasicVSR [1] and BasicVSR++ [2] utilize a bidirectional propagation network and a new alignment scheme is proposed in BasicVSR++. All these methods demonstrate the significance of temporal information for solving the compressed VQE problem.

As far as we know, there is still no real-time compression VQE method that has been proposed so far. The above-mentioned methods cannot be directly applied to webcasting environments due to the limitations of the two real-time issues mentioned above.

Look-up Table. Look-up Tables (LUTs) have proven to be highly effective in reducing computational power and time consumption during the inference phase of algorithms by replacing complex computation processes with simple and fast storage space retrieval operations. Due to its efficient computing advantages, LUTs have been widely utilized for various color transfer tasks such as adjusting image color, exposure, and saturation. And it has been included in the standard profile of the International Color Consortium

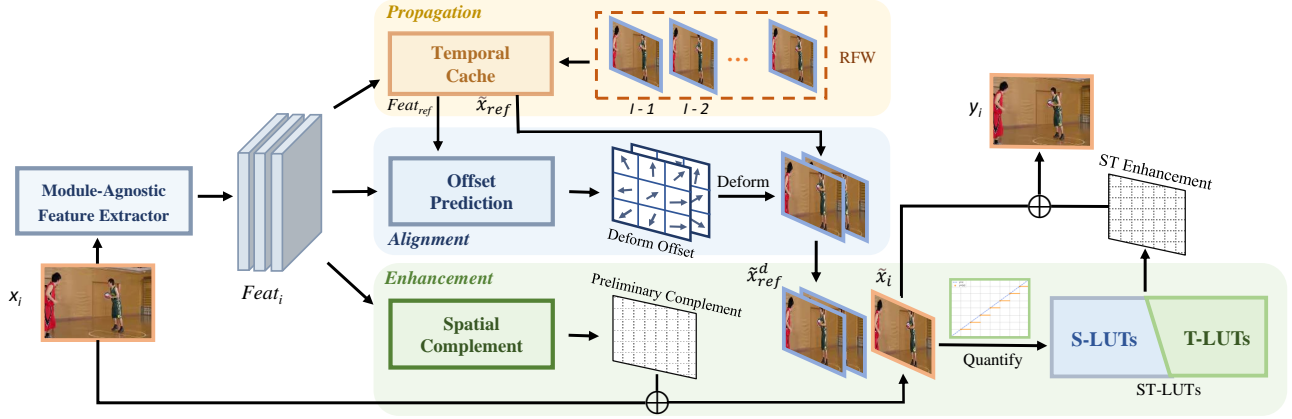


Figure 2. The framework of our proposed method, which consists of a Module-Agnostic Feature Extractor and three main parts: the propagation, alignment and enhancement module. In the inference phase, the propagation module selects the reference frame and accesses the relevant information, which is sent to the alignment module for processing, and finally the aligned and preliminary complemented frames is input to the enhancement module, to obtain the final results.

[24]. However, the use of LUTs directly is not always flexible as it requires manual adjustment by experts to accurately process images. To overcome this limitation, recent attempts have been made to improve LUTs. [27, 33] combine multiple LUTs and learn the weights through neural networks to summing up these LUT results. SR-LUT [13] replaces a small receptive field neural network with a 4D-LUT and achieves good speed-performance trade-offs on super-resolution tasks. SP-LUT [21] and MuLUT [16] makes improvements to the SR-LUT by expanding its receptive field through parallel and serial multiple LUT tables. In this work, we utilize LUTs to extract information in both temporal and spatial dimensions, bringing its advantages to the real-time VQE task.

3. Method

3.1. Overview

Given a stream of compressed frames without an explicit ending frame $\{x_0, x_1, \dots, x_i, \dots\}$, where $x_i \in \mathbb{R}^{C \times H \times W}$ with input channel C , height H and width W , we sequentially enhance each compressed frame to obtain the target sequence $\{y_0, y_1, \dots, y_i, \dots\}$. Due to the low latency requirement of Online-VQE, obtaining information from future frames to enhance x_i is unacceptable. We only use past and current frames $\{x_0, x_1, \dots, x_i\}$ to predict y_i , reducing the video’s delay time. Additionally, to avoid stuttering issues, each frame’s inference speed must be fast enough.

The overall structure of our proposed network is illustrated in Fig. 2. First, a Module-Agnostic Feature Extractor (MAFE) is utilized to extract the feature $Feat_i$ of the current enhancing frame x_i as follows,

$$Feat_i = MAFE(x_i), \quad (1)$$

where the $Feat_i$ will be shared by the three subsequent modules, thus reducing the multiple time-consuming extraction steps and fully exploiting the latent frame feature.

Specifically, in the propagation module, $Feat_i$ is stored in a structure called Temporal Cache, which will provide the temporal information in subsequent modules based on the selection of the reference frames $x_{ref} = \{x_{ref1}, x_{ref2}\}$ without external computation. In the alignment module, $Feat_i$ is concatenate with $Feat_{ref}$, the reference frame feature obtained from the propagation module, to deform x_{ref} with a lightweight offset predictor. In the enhancement module, $Feat_i$ is used to perform a spatial complement, which fully exploits the extracted features and augments the ST-LUTs by increasing its receptive fields.

Under our proposed new framework, only once feature extraction computation for a single frame is required for enhancing each frame. The extracted features are simultaneously computed with reference frame alignment and preliminary compensation in the current frame space.

3.2. The Propagation Module

The propagation module in the VQE task is responsible for extracting and transmitting temporal information within the video. Previous methods have explored various approaches, including designing additional structures [10] and increasing the number of selected reference frames [6, 36] to improve network performance, which greatly increase inference time and computational costs of the model.

The architecture of the propagation module is illustrated in Fig. 3. The compression configuration parameter quantization parameter (QP) value is utilized as an indicator to select fewer but higher quality frames among multiple candidate frames without extra computation. Specifically, a Reference Frame Window (RFW) which contains W frames

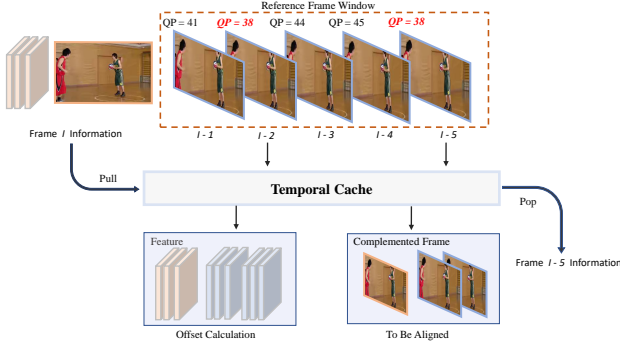


Figure 3. Details of Reference Frame Window and Temporal Cache mechanism in the propagation module.

$\{x_{i-W} \dots x_{i-1}\}$ is set. Then, two frames with the smallest QP values are selected as x_{ref} for the subsequent module.

To mitigate the issue of additional feature extraction operations in previous works, we introduce a cache-like structure known as the Temporal Cache (TC). The TC stores reusable features of past frames that were already extracted by the MAFE in previous process, thereby eliminating the need to re-extract features for each subsequent frame. In particular, when enhancing the i -th frame x_i , STLVQE caches the intermediate feature map $Feat_i$ extracted by the alignment module, as well as the enhanced frame, in the information cache (TC). During reference frame selection, the features and enhanced result of x_{ref1} and x_{ref2} are directly retrieved from TC without extra feature extraction process.

3.3. The Alignment Module

The alignment module is a crucial component in video processing tasks that handles spatial misalignments between frames, which plays a vital role in effectively utilizing the temporal information embedded in the video, especially when the video content is subject to large motion. STLVQE includes a lightweight offset predictor to replace the optical flow or non-local computation of most VQE methods, which significantly reduce the computation cost.

The offset predictor is responsible for predicting spatial offsets which align correlated pixels in the reference with pixels in \tilde{x}_i . As introduced in the last section, the latent features $Feat_{ref}$ and spatially compensated frames \tilde{x}_{ref} at each processing step are stored in TC, which are retrieved by RFW to enhance future frames. Given the feature of a reference frame \tilde{x}_{ref} retrieved from the TC, as well as the feature of the current frame \tilde{x}_i , the offset predictor predicts 9 spatial offsets for each pixel in \tilde{x}_i :

$$o_{ref} = C_{offset}([Feat_i, Feat_{ref}^d]) \quad (2)$$

where the matrix concatenation is denoted by $[\cdot]$, and each offset value in o_{ref} represents the position shift of a correlated pixel in \tilde{x}_{ref} relative to a pixel in \tilde{x}_i .

As shown in Fig. 4, the receptive field for each pixel in the ST-LUTs is 3×3 , which is obtained by rotation ensemble [13] of four 2×2 receptive field kernels, and the corresponding pixels in the reference frames x_{ref} are spatially aligned with the 3×3 pixel offsets o_{ref} and bilinear interpolation. Each set of obtained correlated pixel values of a pixel in \tilde{x}_i are re-arranged into a 3×3 patch, which are then stacked together to obtain the deformed reference frame denoted as \tilde{x}_{ref}^d with the size of $N \times C \times 3H \times 3W$. The final step involves upsampling \tilde{x}_i to match the resolution of \tilde{x}_{ref}^d , then each pixel in the up-sampled \tilde{x}_i^{up} is temporal correlated with the pixel at the same position in \tilde{x}_{ref}^d .

3.4. The Enhancement Module

The enhancement module contains a spatial compensation network and a ST-LUTs network.

To fully utilize the sharing latent feature $Feat_i$, a spatial compensation network reuses $Feat_i$ to generate a spatial residual, which compensates the low quality frame x_i to obtain preliminary spatial enhancement before ST-LUTs:

$$\tilde{x}_i = x_i + C_{comp}(Feat_i) \quad (3)$$

where C_{comp} are 3 shallow convolutional layers. Since the subsequent enhancement module takes the obtained compensated frame \tilde{x}_i as input, spatial compensation network can boost the enhancement performance by expanding the receptive field of the ST-LUTs in the enhancement module.

Instead of deep neural network, STLVQE adopts a novel Spatial-Temporal Look-up Tables in the enhancement module to replace complex float computation with much faster direct memory access, and conducts table queries on both spatial and temporal perspective.

Quantization. Due to the limited storage space of the LUT, the size of each pixel in the input compensated frame \tilde{x}_i^{up} and the deformed frames \tilde{x}_{ref}^d needs to be controlled to fit within a suitable range of bits. Because the range of values in \tilde{x}_i^{up} and \tilde{x}_{ref}^d can vary dynamically and the gradient needs to be passed through the quantization operation during end-to-end training, it's not practical to simply quantize the matrices using a fixed quantization hyper-parameter. The enhancement module adopts a Learnable Quantization layer (LSQ) [9] to quantize the input of the enhancement module, which is the concatenation of \tilde{x}_i^{up} and \tilde{x}_{ref}^d :

$$\begin{aligned} \bar{x} &= [clip(\tilde{x}/s, -Q_N, Q_P)] \\ \hat{x} &= \bar{x} \times s, \end{aligned} \quad (4)$$

where $clip(z, r_1, r_2)$ returns matrix z with values below r_1 set to r_1 and values above r_2 set to r_2 , and the $\lfloor z \rfloor$ rounds z to the nearest integer. The step size parameter s can be optimized along with the network's training. \bar{x} is the indexes used in the LUTs store and retrieval stages, and \hat{x} is a quantized representation of the data with the same scale as x .

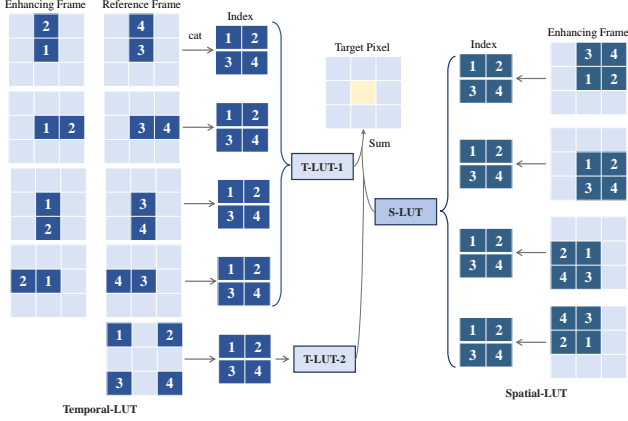


Figure 4. The specific schematic of our Spatial-Temporal Look-up Tables, which consists of two parts: Temporal-LUT (left side) and Spatial-LUT (right side).

After quantization, the deep enhancement network and the corresponding LUTs can be constructed with the quantized pixel values as input.

Deep Enhancement Network Training. In the training phase, a neural network based enhancement module is optimized, which takes the compensated frame \hat{x}_i^{up} and reference frames \hat{x}_{ref}^d as input and output the final enhancement results. To train an enhancement network that is suitable for LUT conversion, the receptive field size of the deep network typically cannot exceed 4. Therefore, each branch of the enhancement network, which will be replaced by ST-LUTs during the inference stage, consists of 1 convolutional layer with a kernel size of 4 and 10 convolutional layers with a 1*1 kernel. The specific design of the network will be illustrated in the appendix.

ST-LUTs Construction. We generate LUTs by permuting all input patches of the receptive field size, and storing all the input/output mappings of the enhancement network in mapping tables. During inference, we retrieve the outputs of the enhancement network directly from the LUTs, replacing slow and computationally resource-intensive floating-point computations with faster memory access. However, due to limited storage space, the number of input-output mappings that can be stored in LUTs is restricted. Typically, a single LUT can only take a 2×2 patch as input. Furthermore, conventional LUTs are not suitable for inter-frame queries in the temporal dimension. To address these issues, we propose the ST-LUTs, which employ multiple LUTs to conduct parallel retrieval with different sets of query pixels in both spatial and temporal dimensions.

Specifically, given the quantized compensated frames \hat{x}_i^{up} and the aligned frames \hat{x}_{ref}^d as input, the look-up tables are constructed as shown in Fig. 4, where two sets of LUTs named S-LUTs and T-LUTs are constructed for extracting spatial and temporal information respectively.

For S-LUTs, a rotation ensemble operation [13] is used during the training process to further expand the LUT receptive field. As shown in Fig. 4, during training, input images are rotated by 0, 90, 180, and 270 degrees, and the results are reverse-rotated and summed up. This approach considers all pixels in a 3×3 receptive field simultaneously. The result of S-LUT R_i^S is expressed as follows:

$$R_i^S = \frac{1}{4} \sum_{j=0}^4 Rot_j^{-1}(f^S(Rot_j(\hat{x}_i^{up}))), \quad (5)$$

where Rot_j and Rot_j^{-1} are the rotation and reserve-rotation operations, and f^S is the spatial enhancement network or the S-LUTs retrieval.

For T-LUTs, the pixels at the same location of the enhancing and reference frames will be strongly correlated after alignment, and jointly considering these values can make full use of the temporal information in the video. As shown on the left in Fig. 4, we establish two T-LUTs: T-LUT-1 take the same position pixels of \hat{x}_i^{up} and \hat{x}_{ref}^d as index with the rotation ensemble operation, while T-LUT-2 uses the four edge pixels of each kernel in the \hat{x}_{ref}^d as indexes to retrieve the surrounding information of the target pixels. The result of T-LUTs R_i^T can be expressed as follows:

$$R_i^{T1} = \frac{1}{4} \sum_{j=0}^4 Rot_j^{-1}(f^{T1}(Rot_j([\hat{x}_i^{up}, \hat{x}_{ref}^d]))), \quad (6)$$

$$R_i^{T2} = f^{T2}(\hat{x}_{ref}^d), \quad R_i^T = R_i^{T1} + R_i^{T2},$$

where f^{T1} and f^{T2} are the temporal enhancement network or the T-LUTs retrieval. Then we can acquire the results of ST-LUTs and get the final enhanced image y_i as follows:

$$R_i = R_i^S + R_i^T, \quad y_i = \tilde{x}_i + R_i. \quad (7)$$

3.5. Training Scheme

We perform the training of the STLVE in two stages with an end-to-end fashion. Firstly, the Charbonnier Loss [3] is utilized to optimize the model as follows:

$$L_{char} = \sqrt{(y_t - \bar{y}_t)^2} + \epsilon, \quad (8)$$

where y_t and \bar{y}_t is the enhanced and ground truth frame at time t , and ϵ is set to 10^{-6} in our paper. Secondly, to further enhance the enhancement capability of the model, we perform fine-tuning using L2 loss with a smaller learning rate as follows:

$$L_{MSE} = \|(y_t - \bar{y}_t)\|_2^2. \quad (9)$$

4. Experiments

4.1. Datasets

Following [6, 10, 36], we conduct our experiments on the MFQE 2.0 dataset. It contains totally 126 sequences videos

Approach	Metrics	High-Latency VQE Methods				Low-Latency VQE Methods									
		MFQE 1.0 [32]		PSTQE [7]		Li et al. [17]		DS-CNN [31]		DnCNN [34]		DCAD [26]		STLVQE(Ours)	
		$\Delta P/\Delta S$	LT/FPS	$\Delta P/\Delta S$	LT/FPS	$\Delta P/\Delta S$	LT/FPS	$\Delta P/\Delta S$	LT/FPS	$\Delta P/\Delta S$	LT/FPS	$\Delta P/\Delta S$	LT/FPS	$\Delta P/\Delta S$	LT/FPS
A	Traffic	0.50/0.90	1120.1	0.64/1.04	5.6K	0.29/0.60	385.5	0.29/0.60	374.6	0.24/0.57	294.9	0.31/0.67	153.7	0.39/0.82	101.9
	PeopleOnStreet	0.80/1.37	1.0	1.08/1.68	0.2	0.48/0.92	2.6	0.42/0.85	2.7	0.41/0.82	3.4	0.50/0.95	6.5	0.65/1.23	9.8
B	Kimono	0.50/1.13		0.69/1.36		0.28/0.78		0.25/0.75		0.24/0.75		0.28/0.78		0.34/0.89	
	ParkScene	0.39/1.03		0.49/1.21	2.9K	0.15/0.48		0.15/0.50		0.14/0.50		0.16/0.50		0.21/0.68	52.2
	Cactus	0.44/0.88	628.1	0.62/1.15	0.4	0.23/0.58	192.8	0.24/0.58	178.2	0.20/0.48	145.4	0.26/0.58	77.5	0.34/0.73	19.2
	BQTerrace	0.27/0.48	2.0	0.50/0.87		0.25/0.48	5.2	0.26/0.48	5.6	0.20/0.38	6.9	0.28/0.50	12.9	0.40/0.74	
C	BasketballDrive	0.41/0.80		0.60/1.04		0.30/0.68		0.28/0.65		0.25/0.58		0.31/0.68		0.45/0.88	
	RaceHorses	0.34/0.55		0.40/0.88		0.28/0.65		0.27/0.63		0.25/0.65		0.28/0.65		0.35/0.90	
	BQMall	0.51/1.03	229.8	0.74/1.44	611.6	0.33/0.88	39.5	0.33/0.80	36.7	0.28/0.68	26.3	0.34/0.88	14.3	0.48/1.11	11.3
	PartyScene	0.22/0.73	10.4	0.51/1.46	1.8	0.13/0.45	25.3	0.17/0.58	27.2	0.13/0.48	38.0	0.16/0.48	69.9	0.26/1.03	88.5
D	BasketballDrill	0.48/0.90		0.66/1.27		0.38/0.88		0.35/0.68		0.33/0.68		0.39/0.78		0.53/1.25	
	RaceHorses	0.51/1.13		0.60/1.44		0.33/0.83		0.32/0.75		0.31/0.73		0.34/0.83		0.38/1.03	
	BQSquare	-0.01/0.15	164.3	0.79/1.14	203.7	0.09/0.25	24.3	0.20/0.38	12.1	0.13/0.18	7.0	0.20/0.38	3.5	0.32/0.66	9.1
	BlowingBubbles	0.39/1.20	32.2	0.62/1.95	7.3	0.21/0.68	41.2	0.23/0.68	82.6	0.18/0.58	142.9	0.22/0.65	285.7	0.30/1.14	109.9
E	BasketballPass	0.63/1.38		0.85/1.75		0.34/0.85		0.34/0.78		0.31/0.75		0.35/0.85		0.44/1.15	
	FourPeople	0.66/0.85		0.95/1.12	1.3K	0.45/0.70		0.46/0.70		0.39/0.60		0.51/0.78		0.66/0.92	
	Johnny	0.55/0.55	345.4	0.75/0.85	0.8	0.40/0.60	87.4	0.38/0.40	81.6	0.32/0.40	64.8	0.41/0.50	34.3	0.58/0.70	24.5
	KristenAndSara	0.66/0.75	4.7	0.93/0.91		0.49/0.68	11.4	0.48/0.60	12.3	0.42/0.60	15.4	0.52/0.70	29.2	0.67/0.74	40.8
	Average	0.46/0.88	-	0.69/1.25	-	0.30/0.66	-	0.30/0.63	-	0.26/0.58	-	0.32/0.67	-	0.44/0.92	-

Table 1. Overall comparison for Δ PSNR(dB), Δ SSIM($\times 10^{-2}$), Latency(ms) and FPS over test sequences of MFQE 2.0 Dataset at QP=37. All methods were retested on a NVIDIA RTX 3090 with the frame-to-frame mode. Video resolution: Class A(2560 \times 1600), Class B(1980 \times 1080), Class C(832 \times 480), Class D(416 \times 240), Class E(1280 \times 720). The High-Latency method cannot be directly applied to the Online-VQE task, and is listed only for performance-speed comparisons.

with multi resolutions: SIF(352 \times 240), CIF(352 \times 288), NTSC(720 \times 486), 4CIF(704 \times 576), 240P(416 \times 240), 360P(640 \times 360), 480P(832 \times 280), 720P(1280 \times 720), 1080P(1920 \times 1080) and WQXGA(2560 \times 1600). Same as [10], the 108 videos in the dataset are used as the training set and 18 videos are used as the test set. All videos were compressed by HM16.5 software in Low Delay P configuration with QP values of 22, 27, 32, 37 and 42.

4.2. Implementation Details

Our proposed network is implemented based on PyTorch framework and MMEediting toolbox [23]. During the training phase, we set batch size to 8 with 180 \times 180 clips from the raw videos and the corresponding compressed videos as training samples. The random flip and rotation augmentation are utilized to fully exploit the information in the samples. The Adam optimizer [14] and Cosine Annealing scheme [19] are utilized for optimizing. The total iterations numbers and initial learning rate of the first and second stages is set to 200K, 1×10^{-4} and 100K, 1×10^{-6} . Our network is trained on 4 Tesla V100 GPUs.

During the inference phase, ST-LUTs will replace the corresponding convolutional layers. To evaluate the model’s performance in an online setting, we conduct inference on the test set frame-by-frame. Following the same settings as [10], we report quality enhancement on Y-channel in YUV/YCbCr space. The Peak Singal-to-Noise Ratio(Δ PSNR) and Structural Similarity(Δ SSIM) will be used as metrics to judge the model’s enhancement capability. We further evaluate the latency(LT) and frame per sec-

Method	LT(ms)	QP37	QP42	QP32	QP27	QP22
RNAN [35]	4329.4	0.44/0.95	-/-	0.41/0.62	-/-	-/-
MFQEv1 [32]	345.4	0.46/0.88	0.44/1.30	0.43/0.58	0.40/0.34	0.31/0.19
MFQEv2 [10]	320.1	0.56/1.09	0.59/1.65	0.52/0.68	0.49/0.42	0.46/0.27
STDF-R1 [6]	85.6	0.65/1.18	-/-	0.64/0.77	0.59/0.47	0.51/0.27
PSTQE [7]	1249.8	0.69/1.25	0.69/1.86	0.67/0.83	0.63/0.52	0.55/0.29
ARCNN [8]	25.1	0.23/0.45	0.29/0.96	0.18/0.19	0.18/0.14	0.14/0.08
DnCNN [34]	64.8	0.26/0.58	0.22/0.77	0.26/0.35	0.27/0.24	0.29/0.18
DS-CNN [31]	81.6	0.30/0.63	0.31/1.01	0.27/0.38	0.27/0.23	0.25/0.15
Li et al. [17]	87.4	0.30/0.66	0.32/1.05	0.28/0.37	0.30/0.28	0.30/0.19
DCAD [26]	34.3	0.32/0.67	0.32/1.09	0.32/0.44	0.32/0.30	0.31/0.19
STLVQE(Ours)	24.5	0.44/0.92	0.46/1.42	0.42/0.65	0.38/0.37	0.31/0.20

Table 2. Latency on 720P video and averaged Δ PSNR/ Δ SSIM comparison on the test sequences of MFQE 2.0 Dataset at different QP values.

ond(FPS) of the models which is crucial to the online-VQE:

$$\begin{aligned}
 LT &= T_{process} + T_{wait}, \\
 T_{wait} &= N_f / FPS,
 \end{aligned}
 \tag{10}$$

where $T_{process}$ refers to the time a model inference a frame and T_{wait} refers to the time required to wait and cache future frames for some video based methods, N_f represent the number of future frames used. Note that the LT metric ignores the frame reception time and decoding time, which is fair for different methods, and we set $FPS=30$ in Eq. 10 as the general online video standard to facilitate comparison.

4.3. Comparison with State of the art Methods

In this subsection, we present the results of our extensive experiments on various QP compressed videos in Tab. 1 and Tab. 2. Our proposed STLVQE network is compared with some widely used or state-of-art single-frame methods [8, 17, 26, 31, 34, 35], as well as some efficient multi-frame methods [6, 7, 10, 32]. Based on a latency thresh-

RFW	TC	DF	PC	$\Delta P/\Delta S$	Time	Params(K)
✓	✓			0.06/0.01	10.85	<1
✓	✓	✓		0.27/0.45	22.30	187
✓	✓		✓	0.39/0.86	21.38	149
✓		✓	✓	0.43/0.92	45.61	233
	✓	✓	✓	0.41/0.87	24.22	233
✓	✓	✓	✓	0.44/0.92	24.51	233

Table 3. Ablation study of Temporal Cache(TC), Reference Frame Window(RFW), Deform Operation(DF), and Preliminary Complement Residual(PC). The latter three sections share the features extracted by MAFE.

old of 100ms for processing 720P video, we have categorized the methods into two groups: high-latency and low-latency approaches. It should be noted that high-latency methods can significantly delay the video, compromising the user’s viewing experience in real-time environments, making them unsuitable for Online-VQE task. We only include these methods in our experiments as a performance upper-bound, and demonstrate our favorable trade-off between performance and inference speed. All experiments were conducted on an NVIDIA RTX 3090 using a frame-to-frame style.

Latency and FPS. Tab. 1 presents the latency and FPS metrics for each VQE approach. We note that while low-latency VQE methods can process each frame at a lower latency and reduce video delay, they often struggle to handle high-resolution videos in real-time, which can lead to stuttering and reduced smoothness. Among the methods listed, only STLVQE can achieve FPS above 40 on 720P resolution videos, making it suitable for most online scenarios. Compared to the second fastest method DCAD, STLVQE’s processing time on 720p video is 9.8 milliseconds faster and outperforms it by a considerable margin, improving PSNR and SSIM metrics by 0.11dB and 0.25×10^{-2} , respectively.

Tab. 2 shows the latency of some large-scale high-latency temporal VQE methods. In contrast, high-latency VQE methods require waiting for future frames or taking a long time for inference, which can cause uncontrollable video delay. The latency of the two high-latency methods in Tab. 1 we evaluated exceeds 400ms, much higher than the latency caused by STLVQE. Moreover, when considering only the FPS metric, STLVQE achieves a significantly faster speed than the single-frame VQE method RNAN(FPS = 0.2) by a factor of 177 on 720P video. Compared with MFQE 1.0, our method is 8.7 times faster. Additionally, STLVQE has a more significant speed advantage on higher resolution videos such as 1080P and 2K.

Enhancement performance. In Tab. 1 and Tab. 2, we present the performance of STLVQE compared to other commonly used or sota VQE methods for each video at QP=37 and for different QP compressed videos, re-

spectively. Our method outperforms all the listed low-latency methods. In comparison with the high-latency VQE method, STLVQE reaches a comparable level with RNAN at QP=37 and QP=32, with only 2.6% and 0.6% of RNAN’s number of parameters and latency time (720P), respectively. The $\Delta SSIM$ of STLVQE is higher than that of the MFQE method for all five QPs, indicating that our method produces an enhanced image with a more stable image structure. The specific visualization results and analysis can be found in *Qualitative Comparison* section. STDF is a robust VQE method, but we believe that a stable latency and higher frame rate are more important for enhancing the user’s viewing experience.

In conclusion, our proposed STLVQE achieves a satisfactory trade-off in terms of speed, latency and enhancement performance, which can be well applied to online scenarios.

4.4. Ablation Study

To validate the effectiveness of our proposed new VQE framework, we perform ablation experiments and specific analysis on three components. The results of the runtime per frame is computed on 720P videos at QP = 37.

Effectiveness of the propagation module. The results are shown in the 4th and 6th row of Table 3. We found that selecting frames based on QP values in RFW can bring a 0.02dB $\Delta PSNR$ performance improvement compared to randomly selecting frames in the RFW, without adding parameters to the network and only increasing the inference time by 0.29ms for comparing QP values of each frame. Furthermore, as shown in rows 5 and 6 of Tab. 3, the use of the TC structure can significantly reduce the inference time by 21.1 ms, which is consumed by the repeated computation of the reference frame information. We achieve this reduction in time by merely occupying the GPU memory with information of several frames in the RFW.

Effectiveness of the alignment module. We mainly validate the effect of the deform operation of the reference frame in the Alignment module. As shown in the first row of Tab. 3, when only using the ST-LUTs structure and discard the whole alignment module and PC operation, the result only has a 0.06 dB PSNR improvement compared to HEVC video. When the Deform operation is applied, the network can capture more accurate temporal information, and the $\Delta PSNR$ reaches 0.27 dB. Due to the lightweight convolutional layers, the alignment module only adds 11.45ms of inference time to the network.

Effectiveness of the enhancement module. As shown in row 3 of Tab. 3, using PC without the Deform operation achieves a significant $\Delta PSNR$ of 0.39 dB, demonstrating the effectiveness of PC in providing initial compensation for spatial information and extending the receptive field, ultimately enhancing the performance of ST-LUTs. Finally,



Figure 5. Qualitative results at QP 37. Video from top to bottom: *BasketballDrive*, *BQMall*, *BQTerrace*, *Kimono*. The STLVQE method successfully enhances the left leg of the athlete, the face of the old man, the railings of the bridge and the eyebrow of the woman in each frame, respectively.

Enhancement Module	$\Delta P/\Delta S$	Time(ms)	Params(K)
S-LUT	0.36/0.83	23.52	233
S-LUT + T-LUT-1	0.37/0.84	24.00	233
ST-LUTs	0.40/0.86	24.51	233
ST-LUTs (on \tilde{x}_i)	0.44/0.92	24.51	233
CNN Network	0.45/0.98	133.25	263

Table 4. Ablation study of STLUTs and the CNN enhancement network. The runtime is computed on a 720P video.

after combining two parts, the network achieves 0.44 dB Δ PSNR. PC alone contributes 0.17 dB to the network and adds only 2.21 ms of inference time.

Tab. 4 provides an analysis of the impact of each LUT in the enhancement module. In the first three rows of the table, we attempted to enhance the original image x_i with the results of different LUT combinations. Results in the first and second rows show that using only the S-LUT with T-LUT-1 does not significantly improve the network due to T-LUT-1 not utilizing all pixels within a kernel when learning the alignment offset. However, when T-LUT-2 is used for network training along with T-LUT-1, the reference frame can be better aligned, resulting in a Δ PSNR improvement of 0.04 dB. The 4th row shows the enhancing result on \tilde{x}_i , reducing the learning difficulty of the ST-LUTs, which improving the performance by 0.03 dB. Compared to the CNN layers replaced by LUTs, ST-LUTs sacrifice only 0.01 dB Δ PSNR performance while reducing the number of param-

eters by 30K and the inference time by 108.74ms.

The above ablation studies have sufficiently demonstrated that the MAFE structure of shared features in STLVQE with the redesigned three new modules can sufficiently reduce the computational redundancy of the network and obtain satisfactory inference speed-performance trade-offs.

4.5. Qualitative Comparison

Fig. 5 provides 4 examples of the qualitative results of our network on compressed video at $QP=37$. The quality of these images deteriorates significantly in compressed scenes, showing a variety of image defects (e.g. blurring of the legs of athletes, missing details in the faces of old man and bridge railings). With the help of temporal information, STLVQE achieves better visual results than single-frame VQE methods with significantly reduced inference time. Compared to large-scale multi-frame VQE methods like MFQE 2.0, STLVQE can achieve competitive capabilities in detail and structural restoration.

5. Conclusion

In this paper, we propose a lightweight and rapid method called STLVQE based on the constraints of online video quality enhancement tasks. STLVQE greatly reduce the computation redundancy and uses a Spatial-Temporal Look-up Table structure to extract spatio-temporal information from the video with minimal time consumption.

The extensive experiments prove that our proposed method can outperform most low-latency VQE methods, achieve competitive performance with high-latency VQE methods which cannot be directly utilized on Online-VQE tasks. Furthermore, STLVQE achieves real-time processing of 720P resolution videos, demonstrating a good trade-off between enhancement performance and inference speed.

References

- [1] Kelvin CK Chan, Xintao Wang, Ke Yu, Chao Dong, and Chen Change Loy. Basicvsr: The search for essential components in video super-resolution and beyond. In *Proceedings of the IEEE/CVF Conference on Computer Vision and Pattern Recognition*, pages 4947–4956, 2021. **2**
- [2] Kelvin CK Chan, Shangchen Zhou, Xiangyu Xu, and Chen Change Loy. Basicvsr++: Improving video super-resolution with enhanced propagation and alignment. In *Proceedings of the IEEE/CVF conference on computer vision and pattern recognition*, pages 5972–5981, 2022. **1, 2**
- [3] Pierre Charbonnier, Laure Blanc-Feraud, Gilles Aubert, and Michel Barlaud. Two deterministic half-quadratic regularization algorithms for computed imaging. In *Proceedings of 1st international conference on image processing*, pages 168–172. IEEE, 1994. **5**
- [4] Honggang Chen, Xiaohai He, Linbo Qing, Shuhua Xiong, and Truong Q Nguyen. Dpw-sdnet: Dual pixel-wavelet domain deep cnns for soft decoding of jpeg-compressed images. In *Proceedings of the IEEE Conference on Computer Vision and Pattern Recognition Workshops*, pages 711–720, 2018. **1, 2**
- [5] Yuanying Dai, Dong Liu, and Feng Wu. A convolutional neural network approach for post-processing in hevc intra coding. In *MultiMedia Modeling: 23rd International Conference, MMM 2017, Reykjavik, Iceland, January 4-6, 2017, Proceedings, Part I 23*, pages 28–39. Springer, 2017. **2**
- [6] Jianing Deng, Li Wang, Shiliang Pu, and Cheng Zhuo. Spatio-temporal deformable convolution for compressed video quality enhancement. In *Proceedings of the AAAI conference on artificial intelligence*, pages 10696–10703, 2020. **1, 2, 3, 5, 6**
- [7] Qing Ding, Liquan Shen, Liangwei Yu, Hao Yang, and Mai Xu. Patch-wise spatial-temporal quality enhancement for hevc compressed video. *IEEE Transactions on Image Processing*, 30:6459–6472, 2021. **2, 6**
- [8] Chao Dong, Yubin Deng, Chen Change Loy, and Xiaoou Tang. Compression artifacts reduction by a deep convolutional network. In *Proceedings of the IEEE international conference on computer vision*, pages 576–584, 2015. **2, 6**
- [9] Steven K Esser, Jeffrey L McKinstry, Deepika Bablani, Rathinakumar Appuswamy, and Dharmendra S Modha. Learned step size quantization. *arXiv preprint arXiv:1902.08153*, 2019. **4**
- [10] Zhenyu Guan, Qunliang Xing, Mai Xu, Ren Yang, Tie Liu, and Zulin Wang. Mfqe 2.0: A new approach for multi-frame quality enhancement on compressed video. *IEEE transactions on pattern analysis and machine intelligence*, 43(3): 949–963, 2019. **1, 2, 3, 5, 6**
- [11] Jun Guo and Hongyang Chao. Building dual-domain representations for compression artifacts reduction. In *Computer Vision–ECCV 2016: 14th European Conference, Amsterdam, The Netherlands, October 11–14, 2016, Proceedings, Part I 14*, pages 628–644. Springer, 2016. **2**
- [12] Zhipeng Jin, Ping An, Chao Yang, and Liquan Shen. Quality enhancement for intra frame coding via cnns: An adversarial approach. In *2018 IEEE International Conference on Acoustics, Speech and Signal Processing (ICASSP)*, pages 1368–1372. IEEE, 2018. **1, 2**
- [13] Younghyun Jo and Seon Joo Kim. Practical single-image super-resolution using look-up table. In *Proceedings of the IEEE/CVF Conference on Computer Vision and Pattern Recognition*, pages 691–700, 2021. **2, 3, 4, 5**
- [14] Diederik P Kingma and Jimmy Ba. Adam: A method for stochastic optimization. *arXiv preprint arXiv:1412.6980*, 2014. **6**
- [15] Dan Kondratyuk, Liangzhe Yuan, Yandong Li, Li Zhang, Mingxing Tan, Matthew Brown, and Boqing Gong. Movinets: Mobile video networks for efficient video recognition. In *Proceedings of the IEEE/CVF Conference on Computer Vision and Pattern Recognition*, pages 16020–16030, 2021. **1**
- [16] Jiacheng Li, Chang Chen, Zhen Cheng, and Zhiwei Xiong. Mulut: Cooperating multiple look-up tables for efficient image super-resolution. In *Computer Vision–ECCV 2022: 17th European Conference, Tel Aviv, Israel, October 23–27, 2022, Proceedings, Part XVIII*, pages 238–256. Springer, 2022. **3**
- [17] Ke Li, Bahetiyaer Bare, and Bo Yan. An efficient deep convolutional neural networks model for compressed image deblocking. In *2017 IEEE International Conference on Multi-media and Expo (ICME)*, pages 1320–1325. IEEE, 2017. **2, 6**
- [18] Ji Lin, Chuang Gan, and Song Han. Tsm: Temporal shift module for efficient video understanding. In *Proceedings of the IEEE/CVF international conference on computer vision*, pages 7083–7093, 2019. **1**
- [19] Ilya Loshchilov and Frank Hutter. Sgdr: Stochastic gradient descent with warm restarts. *arXiv preprint arXiv:1608.03983*, 2016. **6**
- [20] Guo Lu, Wanli Ouyang, Dong Xu, Xiaoyun Zhang, Zhiyong Gao, and Ming-Ting Sun. Deep kalman filtering network for video compression artifact reduction. In *Proceedings of the European Conference on Computer Vision (ECCV)*, pages 568–584, 2018. **1, 2**
- [21] Cheng Ma, Jingyi Zhang, Jie Zhou, and Jiwen Lu. Learning series-parallel lookup tables for efficient image super-resolution. In *Computer Vision–ECCV 2022: 17th European Conference, Tel Aviv, Israel, October 23–27, 2022, Proceedings, Part XVII*, pages 305–321. Springer, 2022. **3**
- [22] Matteo Maggioni, Yibin Huang, Cheng Li, Shuai Xiao, Zhongqian Fu, and Fenglong Song. Efficient multi-stage video denoising with recurrent spatio-temporal fusion. In *Proceedings of the IEEE/CVF Conference on Computer Vision and Pattern Recognition*, pages 3466–3475, 2021. **1**
- [23] MMEediting Contributors. MMEediting: OpenMMLab image and video editing toolbox. <https://github.com/open-mmlab/mmediting>, 2022. **6**

- [24] Matt Pharr and Randima Fernando. *GPU Gems 2: Programming techniques for high-performance graphics and general-purpose computation (gpu gems)*. Addison-Wesley Professional, 2005. 3
- [25] Gary J Sullivan, Jens-Rainer Ohm, Woo-Jin Han, and Thomas Wiegand. Overview of the high efficiency video coding (hevc) standard. *IEEE Transactions on circuits and systems for video technology*, 22(12):1649–1668, 2012. 1
- [26] Tingting Wang, Mingjin Chen, and Hongyang Chao. A novel deep learning-based method of improving coding efficiency from the decoder-end for hevc. In *2017 Data Compression Conference (DCC)*, pages 410–419. IEEE, 2017. 6
- [27] Tao Wang, Yong Li, Jingyang Peng, Yipeng Ma, Xian Wang, Fenglong Song, and Youliang Yan. Real-time image enhancer via learnable spatial-aware 3d lookup tables. In *Proceedings of the IEEE/CVF International Conference on Computer Vision*, pages 2471–2480, 2021. 3
- [28] Thomas Wiegand, Gary J Sullivan, Gisle Bjontegaard, and Ajay Luthra. Overview of the h. 264/avc video coding standard. *IEEE Transactions on circuits and systems for video technology*, 13(7):560–576, 2003. 1
- [29] Yi Xu, Longwen Gao, Kai Tian, Shuigeng Zhou, and Huyang Sun. Non-local convlstm for video compression artifact reduction. In *Proceedings of the IEEE/CVF international conference on computer vision*, pages 7043–7052, 2019. 2
- [30] Ren Yang, Mai Xu, and Zulin Wang. Decoder-side hevc quality enhancement with scalable convolutional neural network. In *2017 IEEE International Conference on Multimedia and Expo (ICME)*, pages 817–822. IEEE, 2017. 1, 2
- [31] Ren Yang, Mai Xu, Tie Liu, Zulin Wang, and Zhenyu Guan. Enhancing quality for hevc compressed videos. *IEEE Transactions on Circuits and Systems for Video Technology*, 29(7): 2039–2054, 2018. 1, 2, 6
- [32] Ren Yang, Mai Xu, Zulin Wang, and Tianyi Li. Multi-frame quality enhancement for compressed video. In *Proceedings of the IEEE conference on computer vision and pattern recognition*, pages 6664–6673, 2018. 2, 6
- [33] Hui Zeng, Jianrui Cai, Lida Li, Zisheng Cao, and Lei Zhang. Learning image-adaptive 3d lookup tables for high performance photo enhancement in real-time. *IEEE Transactions on Pattern Analysis and Machine Intelligence*, 44(4):2058–2073, 2020. 3
- [34] Kai Zhang, Wangmeng Zuo, Yunjin Chen, Deyu Meng, and Lei Zhang. Beyond a gaussian denoiser: Residual learning of deep cnn for image denoising. *IEEE transactions on image processing*, 26(7):3142–3155, 2017. 2, 6
- [35] Yulun Zhang, Kunpeng Li, Kai Li, Bineng Zhong, and Yun Fu. Residual non-local attention networks for image restoration. *arXiv preprint arXiv:1903.10082*, 2019. 6
- [36] Minyi Zhao, Yi Xu, and Shuigeng Zhou. Recursive fusion and deformable spatiotemporal attention for video compression artifact reduction. In *Proceedings of the 29th ACM international conference on multimedia*, pages 5646–5654, 2021. 1, 2, 3, 5